

Controlling three-dimensional magnetic island appearance with external current drive in the Chinese first quasi-axisymmetric stellarator

| | |
|-------|---|
| メタデータ | 言語: en 出版者: IOP Publishing 公開日: 2024-06-17 キーワード (Ja): キーワード (En): 作成者: SU, X., WANG, Xian-Qu, XU, Yuhong, OKAMURA, Shoichi, SHIMIZU, Akihiro, ISOBE, Mitsutaka, CHENG, Jun, LIU, Haifeng, HUANG, Jie, ZHANG, Xin, LIU, Hai, LUO, Y., SHEN, J. F., HU, Jun, TANG, Changjian メールアドレス: 所属: |
| URL | http://hdl.handle.net/10655/0002000635 |

This work is licensed under a Creative Commons Attribution 4.0 International License.



PAPER • OPEN ACCESS

Controlling three-dimensional magnetic island appearance with external current drive in the Chinese first quasi-axisymmetric stellarator







To cite this article: X. Su *et al* 2024 *Nucl. Fusion* **64** 076023

View the [article online](#) for updates and enhancements.

You may also like

- [Suppression of equilibrium magnetic islands by density profile effect in quasi-axisymmetric stellarator plasmas](#)
T Fu, X Q Wang, X Su et al.
- [The three-dimensional equilibrium with magnetic islands and MHD instabilities in the CFQS quasi-axisymmetric stellarator](#)
X.Q. Wang, Y. Xu, A. Shimizu et al.
- [Feasibility study of heavy ion beam probe in CFQS quasi-axisymmetric stellarator](#)
A. Shimizu, M. Isobe, S. Okamura et al.

Controlling three-dimensional magnetic island appearance with external current drive in the Chinese first quasi-axisymmetric stellarator

X. Su¹, X.Q. Wang^{1,*} , Y. Xu¹, S. Okamura² , A. Shimizu^{2,3}, M. Isobe^{2,3}, J. Cheng¹ , H.F. Liu¹ , J. Huang¹ , X. Zhang¹, H. Liu¹ , Y. Luo¹, J.F. Shen¹, J. Hu¹ and C.J. Tang⁴

¹ Institute of Fusion Science, School of Physical Science and Technology, Southwest Jiaotong University, Chengdu 610031, China

² National Institute for Fusion Science, National Institutes of Natural Sciences, Toki, Gifu 509-5292, Japan

³ The Graduate University for Advanced Studies, SOKENDAI, Toki, Gifu 509-5292, Japan

⁴ School of Physical Science and Technology, Sichuan University, Chengdu 610041, China

E-mail: xianquwang@swjtu.edu.cn

Received 20 December 2022, revised 15 May 2024

Accepted for publication 20 May 2024

Published 3 June 2024



Abstract

In this study, the impact of a non-inductive current drive, such as electron cyclotron current drive, on three-dimensional (3D) magnetic islands in the high- β equilibrium of the Chinese First Quasi-axisymmetric Stellarator (CFQS) was investigated using the HINT code. In the case of a high- β equilibrium (volume-averaged plasma beta $\langle\beta\rangle \sim 0.74\%$ and bootstrap current $I_{bs} \sim 24.5$ kA), two $m/n = 4/2$ rational surfaces with large magnetic islands develop (Wang *et al* 2021 *Nucl. Fusion* **61** 036021). The islands can be effectively controlled using a constant or a Gaussian current density profile, depending on the direction and amplitude of the current. With a constant current density amounting to a total current of -6 kA, the rotational transform profile can be modified such that the $m/n = 4/2$ rational surface is eliminated and the island is suppressed. For the Gaussian current density profile, the magnetic island can also be suppressed using a smaller total current of ~ -2 kA to adjust the iota profile. These results suggest that in the CFQS stellarator, the external current drive might be an efficient approach for controlling 3D magnetic islands and consequently improving plasma confinement.

Keywords: quasi-axisymmetric stellarator, magnetic islands, external current drives, CFQS

(Some figures may appear in colour only in the online journal)

* Author to whom any correspondence should be addressed.



Original content from this work may be used under the terms of the [Creative Commons Attribution 4.0 licence](https://creativecommons.org/licenses/by/4.0/). Any further distribution of this work must maintain attribution to the author(s) and the title of the work, journal citation and DOI.

1. Introduction

Magnetic island physics is a major topic of interest in toroidal magnetic confinement devices [1]. The quasi-axisymmetric stellarator (QAS) [2] has been widely studied in the last decades. In the QAS, neoclassical transport properties are similar to those in tokamaks, while there is no requirement of plasma current. Therefore, the QAS is a three-dimensional (3D) tokamak-like device that combines advantages of stellarators and tokamaks [3, 4]. In order to explore the potential merits of the quasi-axisymmetric configuration, several devices with quasi-axisymmetric features have been designed, such as the Compact Helical System (CHS)-qa [5–8], the National Compact Stellarator Experiment (NCSX) [9–11], the Advanced Research Innovation and Evaluation Study-Compact Stellarator (ARIES-CS) [12], the Evolutive Stellarator of Lorraine (ESTELL) [13], a QA developed at New York University [14, 15] and a QA developed at the Max Planck Institute for Plasma Physics (IPP) [16]. Recently, a new QAS device, the Chinese First Quasi-axisymmetric Stellarator (CFQS) has been jointly designed and constructed by Southwest Jiaotong University (SWJTU) and the National Institute for Fusion Science (NIFS). It is a compact stellarator with 16 modular coils that has a major radius of 1 m, toroidal magnetic field of 1 T, toroidal periods of 2, and an aspect ratio of 4 [17–23]. Although stellarator devices do not require plasma current, a substantial bootstrap current is expected in quasi-axisymmetric configurations because of the tokamak-like neoclassical transport behavior, in particular in the high- β operation regime where the finite β and large bootstrap current can excite magnetic islands and overlapping of island chains, limiting the plasma performance [24–27]. More recently, 3D magnetic islands and related stability physics have been investigated for the CFQS [28]. It is found that with bootstrap currents, the low-order islands spread over the whole plasma region, leading to a shrinkage of nested flux surfaces. Therefore, the control of 3D magnetic islands is an important issue for the CFQS stellarator.

On the other hand, in tokamaks the external current drive has been verified as an effective way of replacing the ‘missing’ bootstrap current in the island O -point to stabilize the neoclassical tearing modes (NTMs) and improve plasma confinement [29–32]. In stellarators, an external current drive can be used to control the magnetic configuration [33–35]. Moreover, the capability of current control by the second harmonic electron cyclotron current drive (ECCD) in CFQS has been investigated [23]. The maximum current driven by an electron cyclotron wave power of 400 kW in the optimum beam direction can reach approximately 80 kA. Thus, the application of an external current drive in the CFQS provides a possible means of suppressing 3D magnetic islands as well as ensuring the recovery of good flux surfaces.

In this study, the influence of the external current drive on the control of the $m/n = 4/2$ magnetic islands in the CFQS was studied using the HINT code [24]. The results show that the islands can be effectively suppressed using a constant or Gaussian profile of externally driven currents. It was found that

the change in rotational transform induced by the current drive plays a significant role for the appearance of the 3D magnetic islands in the CFQS device. The remainder of this paper is organized as follows. In section 2, an introduction to the HINT code and the used ‘base’-equilibrium are given. The effects of different current density profiles on 3D magnetic islands are presented in section 3. Finally, section 4 summarizes the results.

2. CFQS equilibrium with islands induced by bootstrap current

The HINT code is a 3D MHD equilibrium calculation code based on the relaxation method for solving the single-fluid nonlinear MHD equations in the right-handed system of cylindrical coordinates (R, ϕ, Z) . It is very different from the VMEC-code, which assumes nested flux surfaces [36]. The VMEC-code is regarded as an effective tool for calculating the 3D MHD equilibrium based on the existence of perfect nested flux surfaces. In the case of low- β equilibria, the VMEC-code is applicable because of the existence of clear flux surfaces. In the case of high- β equilibria, however, the 3D MHD equilibrium can be prone to the generation of magnetic islands and stochastic magnetic fields. Thus, the VMEC-code may be not directly applicable in this case. Compared with the VMEC-code, the advantage of the HINT code is that magnetic surfaces can be destroyed or the magnetic field can develop stochasticization due to the 3D equilibrium response [37]. A detailed introduction to this code has been given in [24]. The new version of the HINT code has high numerical accuracy using a relaxation method based on the equations of the magnetic field \mathbf{B} and of the plasma pressure p [38]. The calculation of the HINT code consists of two processes. The first step is a relaxation process of the plasma pressure to satisfy the condition $\mathbf{B} \cdot \nabla p = 0$ for a fixed \mathbf{B} . The second step is a relaxation process of the magnetic field for a fixed p [24]; the magnetic field is calculated from the artificial dissipative MHD equations as

$$\frac{\partial \mathbf{v}}{\partial t} = -\mathbf{v} \cdot \nabla \mathbf{v} - \nabla p + (\mathbf{j} - \mathbf{j}_0) \times \mathbf{B}, \quad (1)$$

$$\frac{\partial \mathbf{B}}{\partial t} = \nabla \times [(\mathbf{v} \times \mathbf{B}) - \eta(\mathbf{j} - \mathbf{j}_0 - \mathbf{j}_{\text{net}})], \quad (2)$$

$$\mathbf{j} = \nabla \times \mathbf{B}, \quad (3)$$

In the artificial dissipative MHD equations, the plasma pressure p is obtained in the first step, and t is the time, \mathbf{v} is the plasma velocity, \mathbf{j} is the total current density, \mathbf{j}_0 is the coil current density, \mathbf{j}_{net} is a non-vanishing toroidal current density with contributions such as the Ohmic current, the bootstrap current, and the Ohkawa current and others. η is the dissipative parameter and is assumed to be constant. The nonlinear convection term in equation (1) is not considered in the calculation. This two-step calculation process is the basis of the iterative scheme to solve the MHD-equilibrium equations. The final equilibrium state is obtained as an almost stationary steady-state satisfying the force balance $\mathbf{j} \times \mathbf{B} = \nabla p$. This is monitored with the quantities $|\text{d}\mathbf{v}/\text{d}t|^2$ and $|\text{d}\mathbf{B}/\text{d}t|^2$ and the

residual forces which reach in the stationary steady-state sufficiently small levels. In the calculation, the grid number was $128 \times 128 \times 256$ along (R, Z, ϕ) . The box-size was set to $0.3 \text{ m} \leq R \leq 1.6 \text{ m}$, $-0.65 \text{ m} \leq Z \leq 0.65 \text{ m}$, $0 \leq \phi \leq \pi$ in the (R, Z, ϕ) directions, respectively. The artificial resistivity $\eta = 1 \times 10^{-3}$, and the number of steps to solve the MHD equations $n_{\text{stepb}} = 1000$. For the pressure relaxation process mentioned above, the important input parameter L_{in} (length for averaging the pressure along a field line) has been set to 10 m (for details see [24, 37]) which has proved to be numerically sufficient for the size of CFQS.

As is known, the generation of bootstrap currents is inevitable in QAS in particular for high- β operation [19]. The MHD equilibria of CFQS, including the effects of bootstrap current, have been studied in a previous work [28]. For an equilibrium with volume-averaged β values $\langle \beta \rangle \sim 0.74\%$, a bootstrap current of $\sim 24.5 \text{ kA}$ has been calculated for CFQS. This so-called ‘base’-equilibrium is used in this work. In this equilibrium, two $\iota/2\pi = 2/4$ rational surfaces are formed and generate two $m/n = 4/2$ magnetic island-chains, as shown in figure 1.

In this work, we focus on the ‘base’-equilibrium and further study the control of the $4/2$ magnetic islands by the external current drive using the HINT code. The initial pressure profile is set to $p = p_0(1 - s)^2$ to start the HINT computation, where p_0 is the value of the pressure at the magnetic axis and s is the normalized toroidal flux. Figures 1(a) and (c) are the profiles of the rotational transform along the major radius from the magnetic axis to the outboard-side boundary at toroidal angles $\phi = 0^\circ$ and $\phi = 90^\circ$, respectively. We can see that reverse magnetic shear $d\iota/dr < 0$ is produced due to the bootstrap current in the outer part of the plasma. Obviously, there are two $m/n = 4/2$ rational surfaces at normalized minor radius values of $r/a = 0.3$ and $r/a = 0.7$. Figures 1(b) and (d) are the Poincaré plots of magnetic surfaces of the ‘base’-equilibrium at $\phi = 0^\circ$ and $\phi = 90^\circ$, respectively, where the black, blue and red colors mark the regions of $p/p_0 < 1\%$, $1\% \leq p/p_0 \leq 10\%$, and $p/p_0 > 10\%$, respectively. We determine the proxy for the island width using the shown Poincaré plots in the $\phi = 90^\circ$ -plane by measuring the extent of the outboard-side island along the R -axis at $Z = 0$ as shown in figure 1(d) and as indicated there by the double arrow. We note that the start-points for the Poincaré plots begin at the magnetic axis and move outward along the R -axis with a step-size of 0.8 cm. This means that the proxy is a lower limit to the island width since the island separatrix was not determined explicitly. The green line denotes the boundary of the vacuum vessel. The double magnetic island structure without external current drive effect can be seen, and the flux surfaces are destroyed in a manner similar to a double tearing mode in tokamak plasmas [39]. This structure is maintained by the bootstrap current and may lead to a significant limit to the performance of the high plasma beta regime. The existence of a double island structure can be expected to affect the plasma confinement in this configuration. From previous work, it is known that the CFQS rotational transform is characterized by weak magnetic shear and is sensitive to toroidal currents. It is necessary to consider external current drive as one option to adjust the rotational transform

and to control the islands. This may provide a feasible method for the control of the magnetic configuration in CFQS. In this work the bootstrap current is always assumed to be constant and only the current density from the external current drive such as ECCD is varied to study its effects on the equilibrium. In addition, in the HINT calculation process, we use the equilibrium results of the VMEC-code under vacuum conditions as input, and specify the pressure profile and bootstrap current density profile of the ‘base’-equilibrium. Additionally, it should be noted that there may be a limitation in the validity of the present equilibrium study since the bootstrap current used to obtain the ‘base’-equilibrium has been derived under the assumption of an equilibrium consisting of a set of nested flux surfaces calculated with the VMEC-code, thus the bootstrap current is not self-consistent in the various HINT-equilibria. Since the interest is in a situation where good flux surfaces exist again, i.e. the island chains have vanished, the bootstrap current calculations based on nested flux surfaces may have some validity for these cases. However, for the equilibria with island chains the results have to be viewed with caution. When comparing the two cross sections with $\phi = 0^\circ$ and $\phi = 90^\circ$ in figure 1, it is clear that the islands are much better visible at $\phi = 90^\circ$ because of the less shaped flux surfaces. Also, the rotational transform profile along the major radius with $Z = 0$ does show the extent of the resonance more clearly since it passes through the O -points of the islands. Thus, we use in the following section the cross section at $\phi = 90^\circ$ to analyze the dependence of island width and location on the current density profile variations.

3. Effect of the external current drive on islands

3.1. Constant current density profiles

In this section, the current density used for the calculations consists of two parts, the bootstrap current density from the ‘base’-equilibrium and a second one describing the additional current drive, such as constant current density or Gaussian current density. First, we analyze the effect of constant current density profiles $J(\rho) = J_0$, where J_0 is the amplitude of the current density distribution as function of the normalized minor radius $\rho = r/a$, on the double $m/n = 4/2$ island-chains for finite equilibrium- β . In order to separate the externally driven current contribution to the rotational transform profile, we note that the rotational transform can be written as a combination of two terms: $\iota = \iota_p + \Delta \iota$, where ι_p is the rotational transform including beta-effects and the bootstrap current, and $\Delta \iota$ is the contribution to the rotational transform from the additional externally driven current density. Here, the bootstrap current density is kept constant and the externally driven currents, whose effect is studied, are varied. $\Delta \iota(r) = \frac{\mu_0 R I(r)}{2\pi B_\phi r^2}$, with $I(r) = \int_0^{r/a} J(x) x dx$ being the externally driven currents enclosed in the plasma volume of radius r , where x is the variable for integration. The $1/r^2$ dependence, together with CFQS being a low-shear stellarator, make the rotational transform highly sensitive to changes of the toroidal current, such as ECCD.

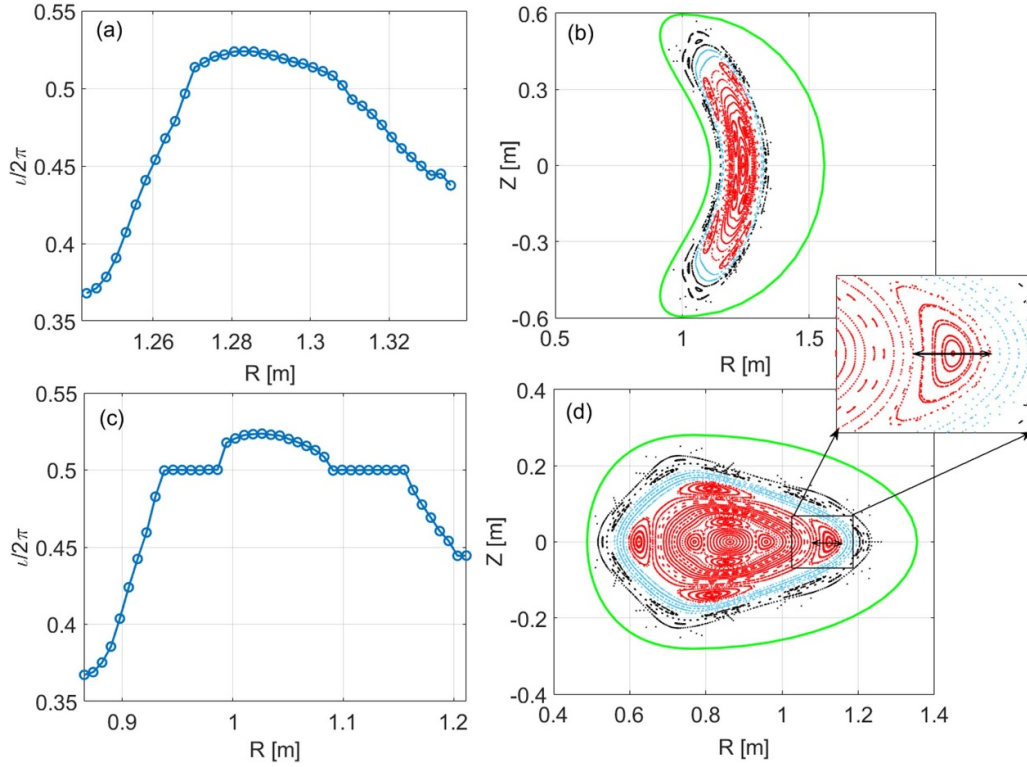


Figure 1. (a)–(b) The radial dependence of the rotational transform and the Poincaré plots of magnetic surfaces at toroidal angle $\phi = 0^\circ$ and (c)–(d) at toroidal angle $\phi = 90^\circ$, respectively, with $\langle \beta \rangle \sim 0.74\%$, $I_{bs} = 24.5$ kA, where the black, blue and red colors mark the regions of $p/p_0 < 1\%$, $1\% \leq p/p_0 \leq 10\%$, and $p/p_0 > 10\%$, respectively. The double arrow denotes the island width in $\phi = 90^\circ$. The green line denotes the boundary of the vacuum vessel.

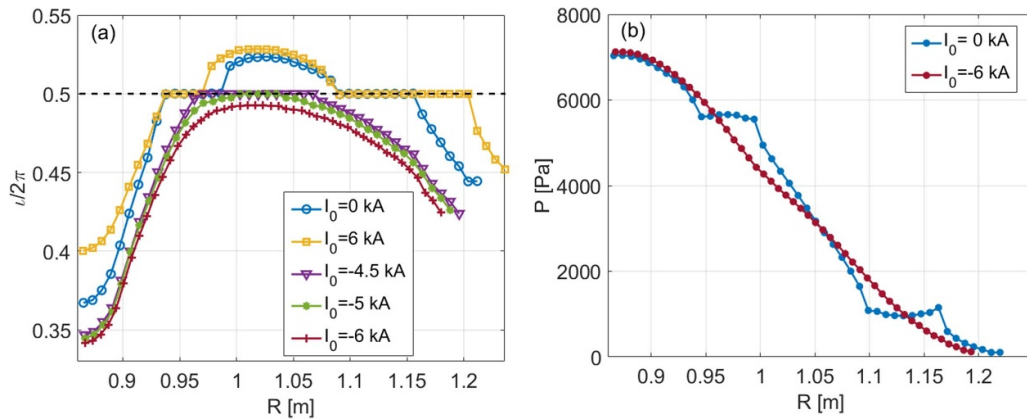


Figure 2. (a) Profiles of the rotational transform with different current amplitudes for constant current density profiles. The black dotted line marks the $m/n = 4/2$ rational surface. (b) Pressure profiles along R with $I_0 = 0$ kA and $I_0 = -6$ kA (with and without islands).

The radial profiles of the rotational transform for different current amplitudes with $-6 \text{ kA} \leq I_0 \leq 6 \text{ kA}$ are depicted in figure 2, where a negative current means the current is in the direction opposite to the direction of ϕ in the cylindrical coordinate system (R, ϕ, Z) . When $I_0 > 0$, $\Delta\iota > 0$ and the rotational transform increases. Conversely $I_0 < 0$, $\Delta\iota < 0$ and the rotational transform decreases. The black dotted line represents the $m/n = 4/2$ rational surface. It was found that when the amplitude of the current is pushed to -6 kA, the rotational transform profile can be changed to eliminate the $m/n = 4/2$ rational surface such that the island is suppressed.

Theoretical estimates can be derived with $I_0 = \int_0^1 J(x) x dx$ and $\Delta\iota_0 = \frac{\mu_0 R I_0}{2\pi B_\phi a^2}$. The values of $\iota(0)$ obtained from the simulated results were compared with the theoretical estimates, where $\iota(0)$ is the rotational transform at the magnetic axis. The parameters of CFQS, namely $B = 1$ T, $R = 1$ m, and $a = 0.25$ m, were employed for our calculations. For the given parameters, the aforementioned estimate of the iota change for a total current of 1 kA with a constant current density results in $\Delta\iota_0 = 0.0032$. Under the ‘base’-equilibrium ($I_0 = 0$ kA) condition, the iota value at the magnetic axis is approximately 0.367. According to the theoretical estimation, if the current

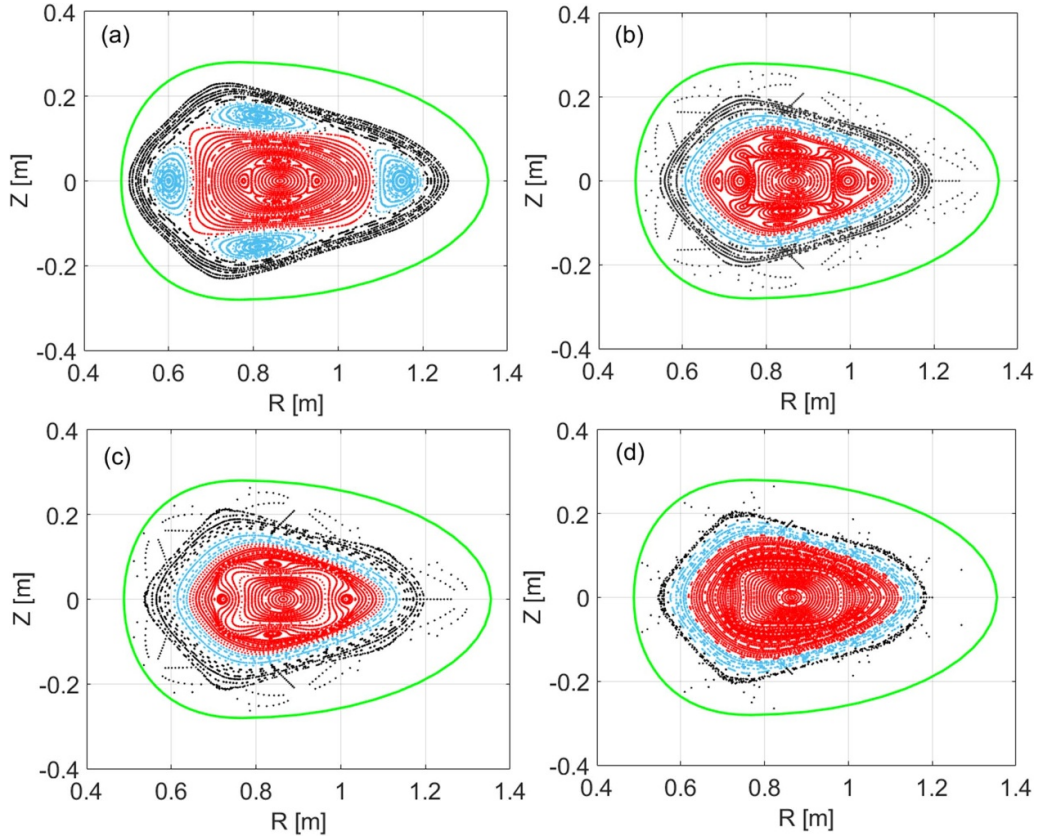


Figure 3. Poincaré plots of the magnetic surfaces with (a) $I_0 = 6$ kA, (b) $I_0 = -4.5$ kA, (c) $I_0 = -5$ kA and (d) $I_0 = -6$ kA.

value is -6 kA, the change in iota is approximately -0.02 . The iota value at the magnetic axis is expected to be 0.0347 , which is consistent with the simulated results ($\iota(0) = 0.342$). The theoretical and simulated results exhibit consistency for current values of -5 kA or -6 kA, owing to the dominant presence of well-defined flux surfaces within the confinement region. The cases with islands do not fit straight-forwardly in such a simple picture since the simple estimate does not account for islands since it is based on nested flux surfaces. In the case of $I_0 = -6$ kA, the rotational transform does not pass through the $m/n = 4/2$ rational surfaces, and both the outer and inner islands are suppressed. This suggests that the radial positions of the magnetic surfaces can be controlled by adjusting the amplitude of the current.

Poincaré plots of the magnetic surfaces with a constant current density profile are depicted in figure 3. When $I_0 = 6$ kA (figure 3(a)), double magnetic islands still exist, and the outer islands are much larger than the inner islands seen in the larger outer resonance region. Figure 3(b) shows the Poincaré plots of the magnetic surfaces with $I_0 = -4.5$ kA. Compared with figure 3(a), we find that the inner and outer islands are close to each other. Note also, the outer islands evolved into island-chains with $m/n = 8/4$ and decreased significantly. This is because the rotational transform profile moves downwards, and leads to coupled double rational surfaces. Interestingly, when $I_0 = -5$ kA, the outer islands nearly disappear, and the inner island width notably decreases. In this case, the outer islands shrink faster than the inner islands. However,

it should be noted that the islands observed in these calculations are not generated by instabilities such as tearing modes, but rather arise from stationary field components resulting from the vacuum field and/or plasma current distributions in connection with a corresponding resonant magnetic surface. When the current increases to $I_0 = -6$ kA as in figure 3(d), the rotational transform profile can be changed to eliminate the $m/n = 4/2$ rational surface so that the island is suppressed for this constant current density case. To understand the change process of the magnetic islands in more detail, we estimate the diameter of the outboard-side island ($R_{\text{island}} > R_{\text{axis}}$) of the island-chain in the $\phi = 90^\circ$ -plane with the O -point located at $Z = 0$ as proxy for the island width (W). In addition, we use the distance from the O -point of the same island to the magnetic axis as the location (D) to illustrate the movement of the magnetic island. In all cases, the radial position of the magnetic axis remains rather constant. We analyzed the W and the D of magnetic islands at different current amplitudes in figure 4. We note that we display in the figures showing the O -point-to-axis distance D only data points with a non-zero island width W . It is found that in the case of a positive current direction, double islands always exist. When the current is increased to ~ 6 kA, there is a partial suppression of the inner islands, but the increase in the outer islands remains. This implies that the outer islands will gradually occupy the entire boundary region as they increase in size with increasing toroidal current values, leading to a reduction in the effective confinement volume. Interestingly, when the direction of the ECCD

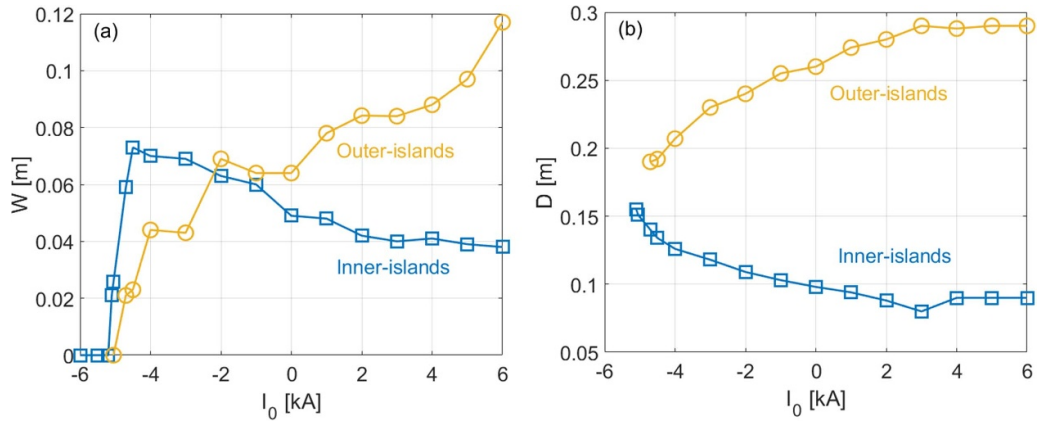


Figure 4. (a) The width of magnetic islands, W , as a function of the current amplitudes I_0 . (b) The distance between the O-point and magnetic axis, as a function of the current amplitude I_0 .

current is reversed, the current can significantly suppress the islands. When the current is sufficiently negative (~ -5 kA), the outer islands almost disappear (red spots). However, the inner islands still exist. With even more negative currents, the outer islands first disappear and then the inner islands disappear. The magnetic configuration has changed from a double island to a single island which refers to the inner island that has not yet completely disappeared. As the current increases, the width of the magnetic islands decreases linearly and finally reaches zero, indicating that the islands vanish completely. However, it is worth noting that although the magnetic island is completely suppressed when the current is large to a certain extent, the structure of $m = 4$ still exists. The $2/4$ -resonance is still rather close to the rotational transform profile. Once a local perturbation results in the rotational transform passing through the $m/n = 4/2$, the magnetic island will reappear. We also find that, when the current changes from 6 kA to -6 kA, the outer islands move towards the magnetic axis while the inner islands stay away from the magnetic axis as shown in figure 4(b), leading to the inner and outer islands becoming closer to each other. They appear to have a competitive relationship, and the inner islands dominate. When the current is about ~ -5 kA, the double rational surfaces become a single rational surface. These are so far the observation with respect to the topological change from two separate $2/4$ -island chains to one $2/4$ -island chain.

3.2. Gaussian current density profiles

In this section, we consider local off-axis heating by the ECCD in the CFQS to further study the effects of local ECCD on the control of 3D magnetic islands. In contrast to the constant current density profile used in section 3.1, a Gaussian current density distribution $J(\rho) = J_0 \exp[-(\rho - \rho_{\text{peak}})^2/\delta]$ is adopted in this case, where ρ_{peak} is the normalized minor radius of the peak position of the current density and δ is the parameter used to adjust the distribution width of the current density. Different current density widths may have a significant effect on the extent of the flat iota-regions of the iota profile, thereby affecting the width of the magnetic island. In the constant current

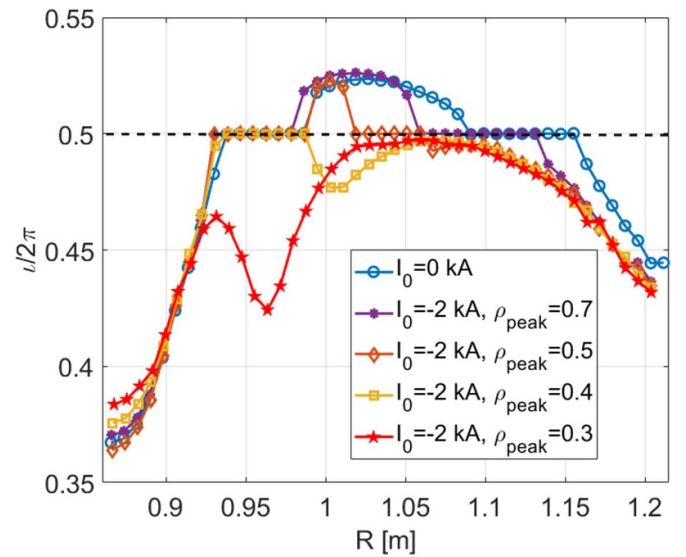


Figure 5. Profiles of the rotational transform with different peak positions of the current. The black dotted line marks the $m/n = 4/2$ rational surface.

density case, additional negative currents preferably showed a suppression of the magnetic islands; thus, only negative additional currents are investigated in this subsection.

The peak position of the current density distribution plays an important role in the suppression dynamics of magnetic islands [29]. First, we discuss the role of the peak position ρ_{peak} of the Gaussian current density distribution in the radial direction with a narrow profile with $\delta = 0.002$. The peak of the externally driven current is chosen to be in the radial range where the rotational transform is close to the rational surfaces. The peak location is varied between the two rational surfaces (inner and outer $4/2$ -resonances) at $R \sim 0.96$ m ($\rho = 0.3$) and $R \sim 1.12$ m ($\rho = 0.7$) with $I_0 = -2$ kA. The profiles of the rotational transform are shown in figure 5. The black dotted line represents the $m/n = 4/2$ rational surface. The results show that in the core and edge regions (far from the deposition location of the ECCD), the current only marginally affects the value of the rotational transform. However,

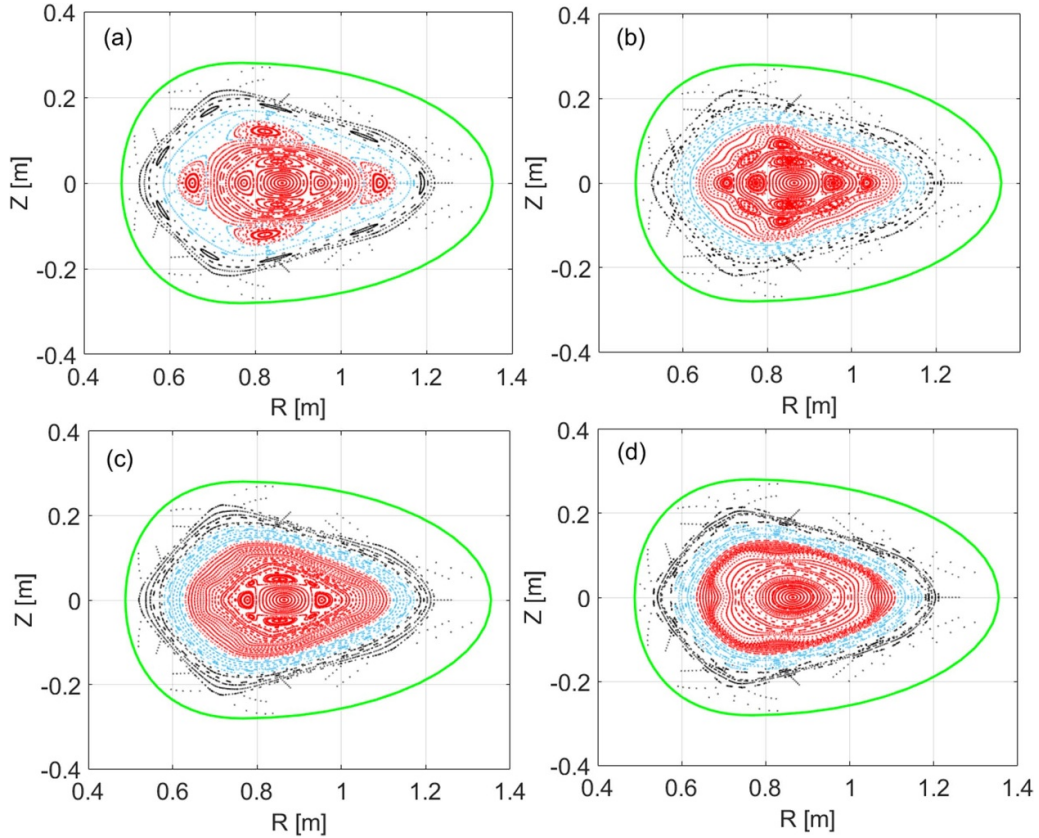


Figure 6. Poincaré plots of magnetic surfaces with different radial peak location ρ_{peak} (a) $\rho_{\text{peak}} = 0.7$, (b) $\rho_{\text{peak}} = 0.5$, (c) $\rho_{\text{peak}} = 0.4$, (d) $\rho_{\text{peak}} = 0.3$.

around ρ_{peak} , the rotational transform is significantly modified. On the one hand, when the position of ρ_{peak} is close to the inner rational surface (case $\rho = 0.3$), a local modification of the rotational transform is noticeable which leads to the disappearance of the $m/n = 4/2$ rational surface. On the other hand, when ρ_{peak} is near the outer rational surface, such as for $\rho_{\text{peak}} = 0.5$ and $\rho_{\text{peak}} = 0.7$, the local variation of the rotational transform is very small at the inner resonance, because the current amplitude varies as $I_0(r) = \int_0^{r/a} J_0 \exp[-(x - \rho_{\text{peak}})^2/\delta] dx$, where x is the variable for integration. Thus, for $\rho_{\text{peak}} = 0.5$ and 0.7 with $\delta = 0.002$, the current at the inner resonance surface ($\rho = 0.3$) is negligibly small. Hence, the inner $m/n = 4/2$ rational surface still exists in these cases. For the case $\rho_{\text{peak}} = 0.3$, the modification of the rotational transform induced by the current is large enough to make the outer island vanish.

The Poincaré plots of equilibria calculated with different radial positions of the peak location ρ_{peak} are shown in figure 6. Figures 6(a)–(d) correspond to $\rho_{\text{peak}} = 0.7, 0.5, 0.4, 0.3$. Comparing the cases with different peak positions of the current density distribution at both the inner and outer rational surfaces, it is found that the islands are completely suppressed when $\rho_{\text{peak}} = 0.3$. However, for $\rho_{\text{peak}} = 0.7$, the islands still exist or have even become larger. In the case of $\rho_{\text{peak}} = 0.5$, the outer $m/n = 4/2$ islands evolve into a $m/n = 8/4$ island-chain. The outer island-chains gradually contract towards the plasma center as ρ_{peak} decreases further. Particularly, when

$\rho_{\text{peak}} = 0.4$, nearly half of the $m/n = 8/4$ structure becomes almost indiscernible, along with corresponding alterations in the plasma current density distribution associated with a resonant magnetic surface. A more detailed variation of the peak-location ρ_{peak} and its effect on the magnetic island width and the distance between the O -point and the magnetic axis is shown in figure 7. For $\rho_{\text{peak}} = 0.7$, the double island-chains structure still exists (see figure 7(a)), with the island width being on the same order as that in the no ECCD case, while the outer islands and the inner islands decrease in size as ρ_{peak} approaches the inner rational surface. We also find that when $\rho_{\text{peak}} = 0.38$, the outer islands disappear and the double island topology changes to a single island topology, and with a further decrease of ρ_{peak} the inner islands width decreases. Further, the outer islands move toward the magnetic axis, but the inner islands move only slightly as shown in figure 7(b). In this process, the double $m/n = 4/2$ island-chain transforms to a single island-chain. It is also worth noting that in the regimes of $\rho_{\text{peak}} \leq 0.4$ the width of the islands decreases quickly until the islands are completely suppressed as $\rho_{\text{peak}} \sim 0.3$ in which a deeper local minimum in the rotational transform profile is formed around ρ_{peak} . Therefore, it can be concluded that in the reversed magnetic shear configuration, the suppression of the 3D magnetic island is more efficient for ρ_{peak} further inside than for ρ_{peak} further outside.

In the case of the constant current density, the amplitude of the current is an important parameter for the suppression

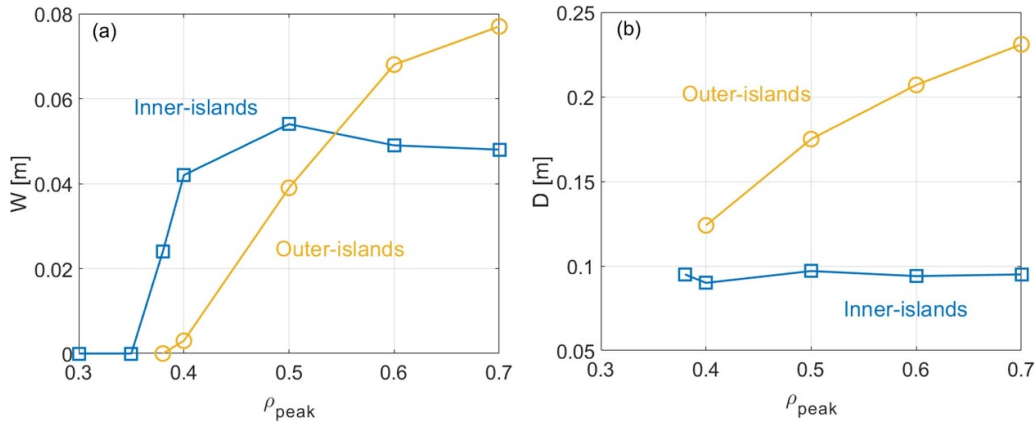


Figure 7. (a) The width of magnetic islands W as a function of radial peak location ρ_{peak} . (b) The distance between O-point and magnetic axis D as a function of radial peak location ρ_{peak} .

of islands. To investigate the control of an $m/n = 4/2$ island in detail, we further studied the influence of the current amplitude on the islands for $\rho_{\text{peak}} = 0.3$ and $\delta = 0.002$. The rotational transform profiles as a function of the current amplitude are shown in figure 8. The simulation results show that the rotational transform is highly sensitive to the amplitude of the current. As already shown, when $I_0 = -2$ kA, the rotational transform profile can be changed to eliminate the $m/n = 4/2$ rational surface. It should be noted that exceeding an amplitude of -2 kA for the current, such as -3 kA or -4 kA, leads to a significant variation in the rotational transform and induces the generation of numerous additional rational surfaces, such as $m/n = 5/2$, which are located close to the axis and have the potential to generate a core magnetic island. It can also cause the overlap of multiple magnetic islands between different rational surfaces as a result of toroidal coupling. Therefore, controlling the current amplitude via the ECCD power level may also be crucial to avoid adverse effects in the suppression of the magnetic islands in CFQS.

Poincaré plots of the magnetic surfaces with different current amplitudes are shown in figure 9. With the increase of the current amplitude, the island chain appearance changes from a double island structure to a single island structure, and finally the magnetic islands are completely suppressed when $I_0 = -2$ kA. It is worth noting that when $I_0 = -1.5$ kA, the outer island chain becomes a chain with high- n but small islands. The width of the magnetic islands and the distance between the O-point and the magnetic axis with different currents are shown in figure 10. As the current amplitude increases, the width of the outer islands decreases because of the inward movement of the outer rational surface. The width of the inner islands reaches a maximum at $I_0 = -1.5$ kA, and then reduces to zero. The double island chain persists until the current amplitude reaches -1.7 kA, and the reduction of the island width in the single island state depends almost linearly on the change in the current amplitude. Figure 10(b) also shows that the distance D has a similar dependence on I_0 when comparing with figure 4(b), while the change of the current amplitude ($-2 \text{ kA} < I_0 < 0$) is much smaller than that for the constant current density scan.

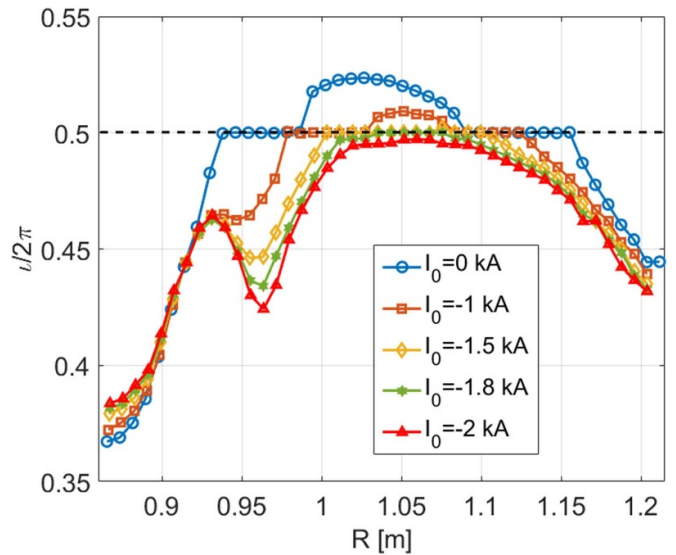


Figure 8. Profiles of the rotational transform for different current amplitudes. The black dotted line is the $m/n = 4/2$ rational surface.

Moreover, a different width of the current density may also affect the extent of the small-shear iota-regions between the two $m/n = 4/2$ rational surfaces thereby affecting the width of the magnetic islands. In this part of the section, we consider this effect on the 3D magnetic islands by changing $\delta = 0.002, 0.065, 0.1, 0.3$ with $I_0 = -2$ kA at $\rho_{\text{peak}} = 0.3$. From figure 11, owing to the changes of deposition width, the magnetic shear near the peak position of the current density is modified. When the current density width becomes narrower, the change in the iota-profile gets stronger and therefore the rational surfaces move away from the current density peak location. And when $\delta = 0.002$, the $m/n = 4/2$ rational surface is eliminated from the rotational transform profiles. As the Gaussian current density profile tends to flatten, the island width increases and there is no suppression of the islands.

In figure 12, Poincaré plots exemplify the results for different δ . A small island-chain with high- n is dimly visible in the core plasmas, such as a $9/4$ island-chain. However, we did

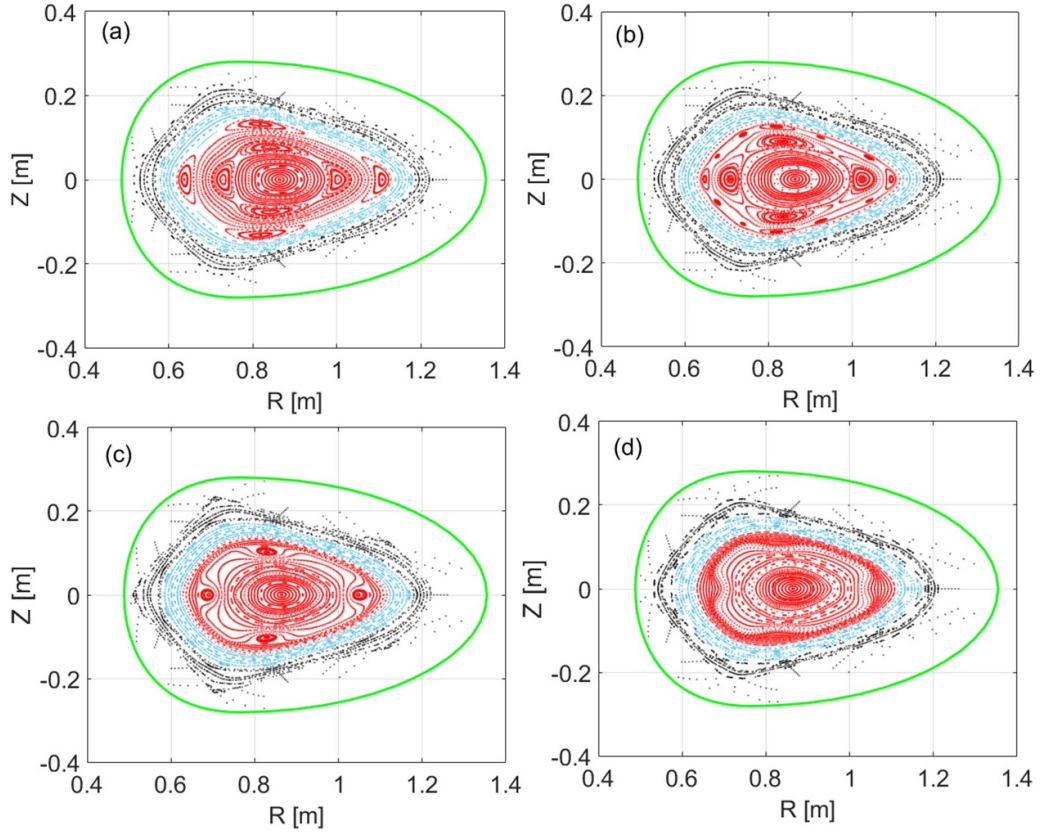


Figure 9. Poincaré plots of magnetic surfaces with different current amplitude (a) $I_0 = -1$ kA, (b) $I_0 = -1.5$ kA, (c) $I_0 = -1.8$ kA, and (d) $I_0 = -2$ kA.

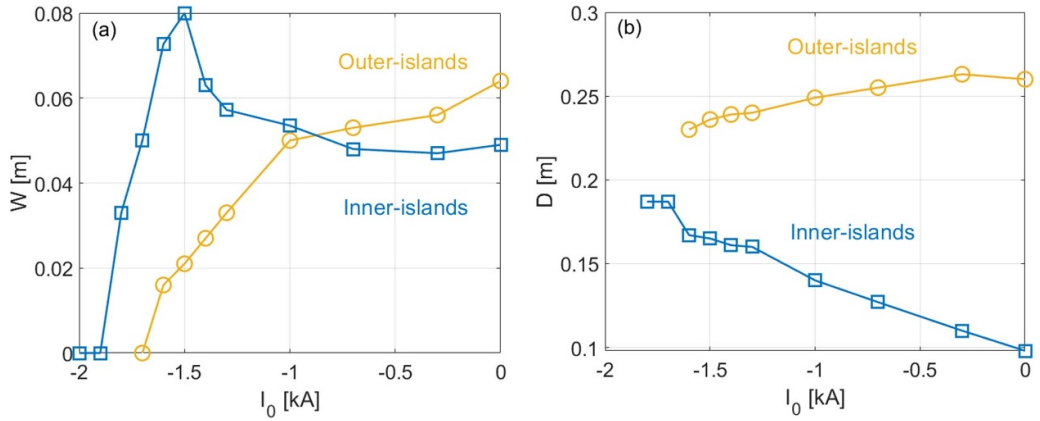


Figure 10. (a) The width of magnetic islands as a function of the amplitude of current I_0 . (b) The distance between the O-point and magnetic axis as a function of the amplitude of current I_0 .

not find a 8/4-island chain like in figure 6 or 9 in the investigated cases. In the case of $\delta = 0.1$ (figure 12(b)), we found that, where the X-points of the islands are expected, the flux surfaces from the region inside the double island region bulge outward in an interchange-like structure. When $\delta = 0.065$, the inner island has moved outward and is almost vanishing (figure 12(c)). When the width of the current density is small enough, the outer islands also shrink and generate good flux surfaces finally. Figure 13(a) shows the dependence of the width of the islands on the radial width of the Gaussian current

density profile. It is found that the island width decreases with decreasing values of δ , particularly for the inner islands. Once $\delta < 0.1$, the island is suppressed quickly and disappears when $\delta = 0.002$. For $\delta > 0.1$, the island width saturates. For the large δ regime with $\delta > 0.3$, corresponding to the flat current density profile, the island width is also close to the result of the constant current density with $I_0 \sim -2$ kA. This suggests that the magnetic islands can be suppressed more effectively in the case of a narrow current density form like for $\delta = 0.002$, $I_0 = -2$ kA and $\rho_{\text{peak}} = 0.3$. Also, in figure 13(b),

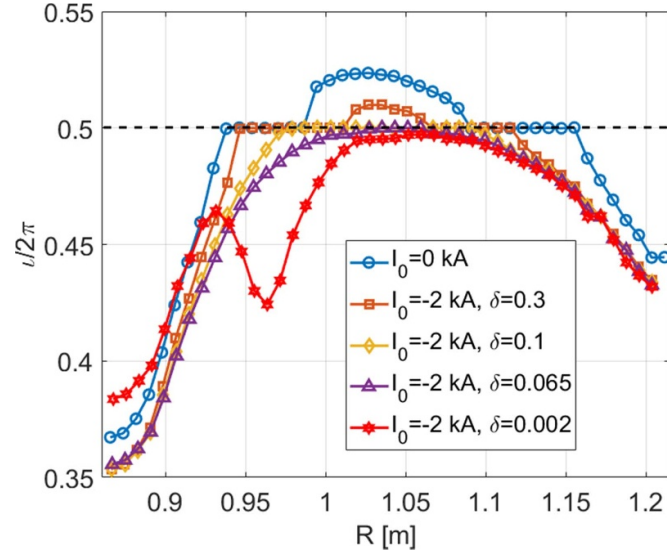


Figure 11. The rotational transform for different values of δ . The black dotted line is $m/n = 4/2$ rational surface.

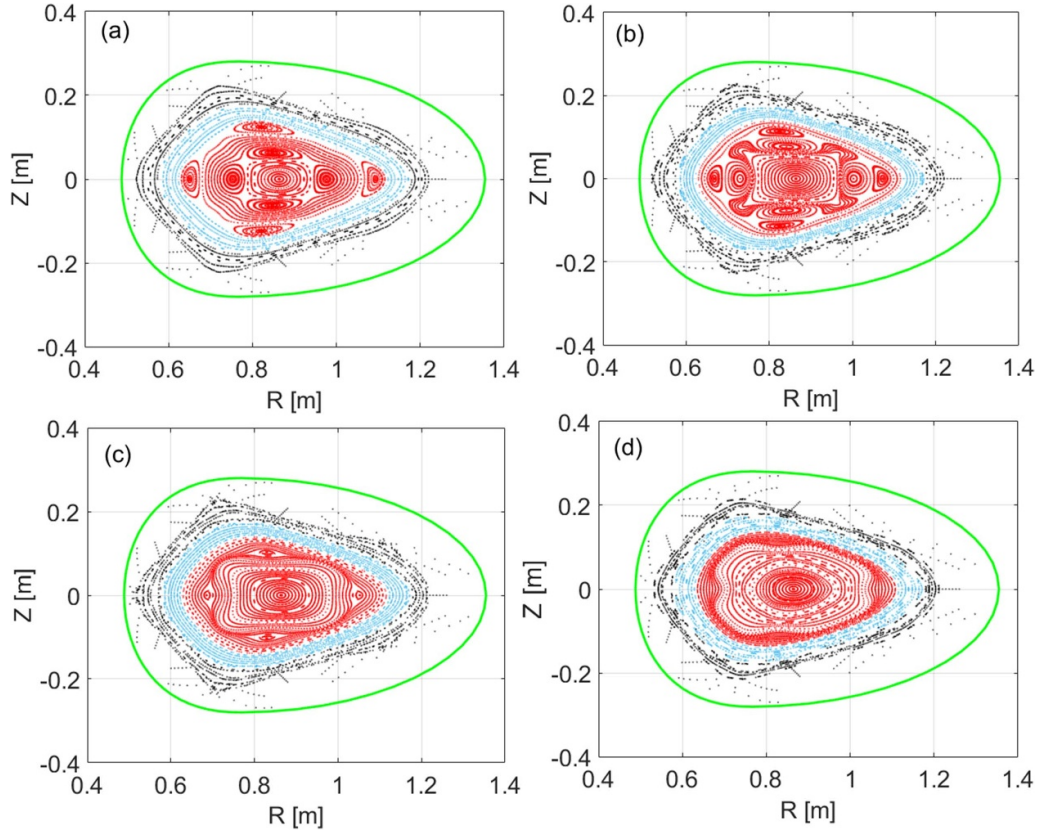


Figure 12. Poincaré plots of magnetic surfaces of calculations with different δ , (a) $\delta = 0.3$, (b) $\delta = 0.1$, (c) $\delta = 0.065$, and (d) $\delta = 0.002$.

as δ increases, the inner island locations move toward the core, and the outer island locations move toward the boundary. However, as the value of δ decreases, the island chain undergoes a reduction in size, and at $\delta = 0.065$, the inner magnetic island is almost completely suppressed. This also provides a knob to control the inner or outer islands in the CFQS.

4. Summary

In this work, we applied the HINT code to study the impact of a non-inductive current drive on the 3D magnetic islands generated in the high- β operation of the CFQS stellarator. The results show that the islands can be significantly suppressed using a constant or Gaussian profile of an externally driven current,

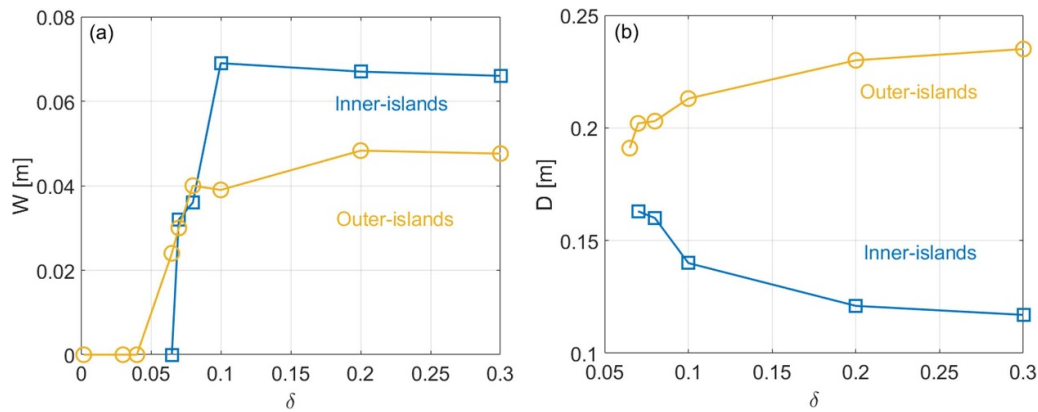


Figure 13. The width of magnetic islands W and the distance between O-point and magnetic axis as a function of δ .

depending on the direction and amplitude of the applied current. The control of magnetic islands with different parameters of the profile of the driven currents was investigated in detail. The main results are summarized as follows: For a constant externally driven current profile, values of -6 kA are sufficient to eliminate the $m/n = 4/2$ rational surface from the rotational transform profile and to suppress the islands. When the direction of the driven current is reversed, the rotational transform profile is strongly modified, passing through the rational surface with $\iota/2\pi = 0.5$, resulting in the width of the outer islands being significantly larger than those of the inner islands. In the case of Gaussian current-driven profiles, the radial location (ρ_{peak}) of the peak current density, the amplitude (I_0) and width (δ) of the driven current all play significant roles in controlling or suppressing the magnetic island-chains. It was found that (i) the islands can be completely suppressed when $\rho_{\text{peak}} = 0.3$ with $\delta = 0.002$ and a current amplitude of -2 kA; (ii) For a broader current density with $\delta > 0.04$ or for the peak position moving towards the boundary as for the cases with $\rho_{\text{peak}} > 0.3$, the $m = 4$ $n = 2$ rational surface still exists and the magnetic island cannot be completely suppressed for the fixed current amplitude $I_0 = -2$ kA. The above results suggest that in the CFQS stellarator the external current drive might be an effective means for controlling 3D magnetic islands and may help to improve the plasma confinement. It should be noted that the results demonstrated above were obtained with a not-self-consistent bootstrap current profile. As a result of it, the parameters necessary to suppress the islands will have to be adapted according to the experimental results. Additionally, at present, the applied parameter range of the constant and Gaussian distributed current density is limited. Extension of the parameter range will be done in the near future.

Acknowledgments

The authors would like to thank Professor Y Suzuki for the HINT code. This work was supported by the National Key R&D Program of China under Grant Nos. 2022YFE03070000, 2022YFE03070001, 2019YFE03020002 and the National Natural Science Foundation of China under Grant No.

U22A20262, and the Science and Technology Plan Project in Sichuan Province of China under Grant No. 2022JDJQ0036, and NIFS international collaborations with overseas laboratories (UFEX105), and NIFS promotion of magnetic confinement research using helical devices in Asia (URSX108), and the NIFS general collaboration project, NIFS18KBAP041, NIFS20KBAP067, NIFS20KBAE001, NIFS22KIPH009, NIFS22KIPH011 and NIFS22KIEE001, and ‘PLADyS’, JSPS Core-to-Core Program, A. Advanced Research Networks.

ORCID iDs

X.Q. Wang <https://orcid.org/0000-0001-8485-895X>
 S. Okamura <https://orcid.org/0000-0002-8156-8233>
 J. Cheng <https://orcid.org/0000-0002-0496-5542>
 H.F. Liu <https://orcid.org/0000-0002-0424-645X>
 J. Huang <https://orcid.org/0000-0003-4179-943X>
 H. Liu <https://orcid.org/0000-0001-6407-5958>

References

- [1] Narihara K. et al 2001 *Phys. Rev. Lett.* **87** 135002
- [2] Nuehnenberg J. et al 1994 Quasi-axisymmetric tokamaks *Theory of Fusion Plasmas Proc. Joint Varenna-Lausanne Int. Workshop* (Editrice Compositori) pp 3–12
- [3] Feng Z.C., Gates D.A., Lazerson S.A., Landreman M., Pomphrey N. and Fu G. 2020 *Phys. Plasmas* **27** 022502
- [4] Landreman M. and Paul E. 2022 *Phys. Rev. Lett.* **128** 035001
- [5] Okamura S. et al 2000 *J. Plasma Fusion Res. Ser.* **3** 73
- [6] Okamura S. et al 2001 *Nucl. Fusion* **41** 1865
- [7] Matsuoka K. et al 2004 *Fusion Sci. Technol.* **46** 378
- [8] Okamura S. et al 2004 *Nucl. Fusion* **44** 575
- [9] Reiman A. et al 1999 *Plasma Phys. Control. Fusion* **41** B273
- [10] Neilson G.H. et al 2000 *Phys. Plasmas* **7** 1911
- [11] Zarnstorff M.C. et al 2001 *Plasma Phys. Control. Fusion* **43** A237
- [12] Najambadi F. et al 2008 *Fusion Sci. Technol.* **54** 655
- [13] Drevlak M. et al 2013 ESTELL: a quasi-toroidally symmetric stellarator *Contrib. Plasma Phys.* **53** 459–68
- [14] Garabedian P.R. 2008 *Proc. Natl Acad. Sci. USA* **105** 13716
- [15] Garabedian P.R. et al 2009 *J. Res. Natl Inst. Stand. Technol.* **114** 229

- [16] Henneberg S., Drevlak M., Nührenberg C., Beidler C.D., Turkin Y., Loizu J. and Helander P. 2019 *Nucl. Fusion* **59** 026014
- [17] Liu H. *et al* 2018 *Plasma Fusion Res.* **13** 3405067
- [18] Liu H. *et al* 2021 *Nucl. Fusion* **61** 016014
- [19] Shimizu A. *et al* 2018 *Plasma Fusion Res.* **13** 3403123
- [20] Shimizu A. *et al* 2021 *Nucl. Fusion* **62** 016010
- [21] Isobe M. *et al* 2019 *Plasma Fusion Res.* **14** 3402074
- [22] Kinoshita S., Shimizu A., Okamura S., Isobe M., Xiong G., Liu H. and Xu Y. (CQFS Team) 2019 *Plasma Fusion Res.* **14** 3405097
- [23] Yoshimura Y. *et al* 2022 *Plasma Fusion Res.* **17** 2402039
- [24] Suzuki Y., Nakajima N., Watanabe K., Nakamura Y. and Hayashi T. 2006 *Nucl. Fusion* **46** L19
- [25] Suzuki Y. and Geiger J. 2016 *Plasma Phys. Control. Fusion* **58** 064004
- [26] Knieps A. *et al* 2021 *Nucl. Fusion* **62** 026011
- [27] Zhou S. *et al* 2022 *Nucl. Fusion* **62** 106002
- [28] Wang X.Q. *et al* 2021 *Nucl. Fusion* **61** 036021
- [29] La Haye R.J., Günter S., Humphreys D.A., Lohr J., Luce T.C., Maraschek M.E., Petty C.C., Prater R., Scoville J.T. and Strait E.J. 2002 *Phys. Plasmas* **9** 2051–60
- [30] Zohm H. *et al* 1999 *Nucl. Fusion* **39** 577
- [31] Gantenbein G., Zohm H., Giruzzi G., Günter S., Leuterer F., Maraschek M., Meskat J. and Yu Q. (ASDEX Upgrade Team) 2000 *Phys. Rev. Lett.* **85** 1242
- [32] Hegna C.C. and Callen J.D. 1997 *Phys. Plasmas* **4** 2940–6
- [33] Reiman A.H. 1983 *Phys. Fluids* **26** 1338–40
- [34] Lopez-Bruna D. *et al* 2014 *CIEMAT* p 1333
- [35] Geiger J., Beidler C.D., Drevlak M., Maaßberg H., Nührenberg C., Suzuki Y. and Turkin Y. 2010 *Contrib. Plasma Phys.* **50** 770–4
- [36] Hirshman S.P. and Whitson J.C. 1983 *Phys. Fluids* **26** 3553
- [37] Suzuki Y. 2017 *Plasma Phys. Control. Fusion* **59** 054008
- [38] Suzuki Y. 2020 *Plasma Phys. Control. Fusion* **62** 104001
- [39] Bierwage A., Benkadda S., Hamaguchi S. and Wakatani M. 2005 *Phys. Plasmas* **12** 082504